The Cryosphere Discuss., 7, 2373–2412, 2013
www.the-cryosphere-discuss.net/7/2373/2013/
doi:10.5194/tcd-7-2373-2013

The Cryosphere Discussions
Open Access

Solving Richards Equation for snow improves snowpack meltwater runoff estimations

N. Wever[1], C. Fierz[1], C. Mitterer[1], H. Hirashima[2], and M. Lehning[1,3]

[1]WSL Institute for Snow and Avalanche Research SLF, Flüelastrasse 11, 7260 Davos Dorf, Switzerland
[2]Snow and Ice Research Center, NIED, Japan
[3]CRYOS, School of Architecture, Civil and Environmental Engineering, EPFL, Lausanne, Switzerland

Received: 25 April 2013 – Accepted: 29 April 2013 – Published: 5 June 2013

Correspondence to: N. Wever (wever@slf.ch)

Published by Copernicus Publications on behalf of the European Geosciences Union.

Abstract

The runoff from the snow cover during spring snow melt or rain-on-snow events is an important factor in the hydrological cycle. In this study, water transport schemes for a 1-dimensional physical based snowpack model are compared to 14 yr of lysimeter measurements at a high alpine site. The schemes include a simple bucket-type approach, an approximation of Richards Equation (RE), and the full RE. The results show that daily sums of runoff are strongly related to a positive energy balance of the snow cover and therefore, all water transport schemes show very similar performance in terms of Nash–Sutcliffe efficiency (NSE) coefficients (around 0.59) and r^2 values (around 0.77). Timing of the arrival of meltwater in spring at the bottom of the snowpack showed differences between the schemes, where especially in the bucket-type and approximated RE approach, meltwater release is slower than in the measurements. Overall, solving RE for the snow cover yields the best agreement between modelled and measured runoff. On sub-daily time scales, the water transport schemes behave very differently. Also here, solving RE provides the highest agreement between modelled and measured runoff in terms of NSE coefficient (0.48), where other water transport schemes loose any predictive power. This appears to be mainly due to bad timing of meltwater release during the day. Accordingly, solving RE for the snow cover improves several aspects of modelling snow cover runoff. The additional computational cost was found to be in the order of a factor of 1.5.

1 Introduction

The presence of a snow cover has a strong impact on the hydrological cycle. The snow cover can delay the routing from precipitation to streamflow on time scales from a few hours or days to several months and many studies have shown the importance of the snow cover for accurate runoff and streamflow modelling (e.g., Seyfried et al., 2009; Koster et al., 2010; Mahanama et al., 2012). Furthermore, the effects of rain-on-snow

TCD
7, 2373–2412, 2013

(ROS) events on runoff from catchments is strongly dependent on the state of the snow cover (Marks et al., 2001; Mazurkiewicz et al., 2008). For this reason, the use of physical based snowpack models for hydrological modelling is increasing, with varying degrees of model complexity. Studies have shown that using physical based snowpack models improves the determination of (spatial distribution of) snow water equivalent and discharge at basin outlets (Marks et al., 1999; Zanotti et al., 2004). A correct description of water flow through a snowpack is not only important to improve meltwater runoff estimations, but also helps to improve understanding wet snow avalanche formation (Conway and Raymond, 1993; Mitterer et al., 2011).

One of the couplings between the snow cover and surface or sub-surface flow is provided by meltwater runoff at the base of the snowpack. For an accurate assessment of the snowpack meltwater runoff, it is important to have a good understanding of water movement through a snowpack. Water transport in snow is a complex process, because in general, the snow cover consists of many layers that vary in temperature, grain size and type and density. Experimental studies have shown that microstructural properties of the snowpack strongly influence the hydraulic properties of snow (Shimizu, 1970; Colbeck, 1974; Marsh, 1991; Yamaguchi et al., 2010). Where a snow layer with small grains is on top of a layer with course grains, these differences in hydraulic properties will lead to the formation of capillary barriers at the interface (Jordan, 1996; Waldner et al., 2004; Peitzsch et al., 2008; Mitterer et al., 2011). Also lateral flow along these capillary barriers or ice lenses or other dense parts of the snow cover has been identified (Peitzsch et al., 2008). Field experiments also have repeatedly observed the existence of preferential flow paths, which can provide a more efficient water transport mechanism than matrix flow alone (e.g., Kattelmann, 1985; Schneebeli, 1995; Katsushima et al., 2013).

For modelling of the snow cover, capillary effects are often neglected and many models follow a bucket-type approach (e.g., Jin et al., 1999; Marks et al., 1999; Boone and Etchevers, 2001). These water transport schemes are easy to implement and computationally very efficient, making them very suitable for distributed modelling. Richards

TCD
7, 2373–2412, 2013

Equation (Richards, 1931), hereafter denoted as RE, is often applied to soils to describe variably saturated matrix flow. However, its potential to apply for snow covers as well has already been identified in literature (Colbeck, 1972, 1974; Jordan, 1983; Illangasekare et al., 1990; Hirashima et al., 2010). Jordan (1996) and Hirashima et al. (2010) found that RE was able to reproduce the formation of capillary barriers as observed in laboratory experiments and snow profiles.

Compared to the knowledge of hydraulic properties in various types of soil, measurements to derive hydraulic properties in natural snow has been restricted to a few studies (Shimizu, 1970; Colbeck, 1974; Marsh, 1991; Yamaguchi et al., 2010). Except for the study by Colbeck (1974), these studies were focussed on wet snow. Other snow types are more difficult to investigate, because in the presence of liquid water, snow metamorphism is rapid.

Several snowpack models that describe liquid water transport on the basis of RE have been developed. Some model studies were restricted to idealized snowpacks to quantify the effects of water percolation in snow (Illangasekare et al., 1990; Jordan, 1996; Daanen and Nieber, 2009). Gravitational flow resulting from RE, as proposed by Colbeck (1972) has been used in CROCUS (Brun et al., 1989) and SNTHERM (Jordan, 1991; Davis et al., 2001). To our knowledge, the full RE has not been used in a physical based snow cover model for simulating complete snow seasons based on meteorological field measurements. In this study, the implementation of a solver for RE in the physical based snowpack model SNOWPACK (Bartelt and Lehning, 2002; Lehning et al., 2002a,b) is described, where the snowpack and soil are treated as a continuous column. Using this model, 14 snow seasons are modelled for a high alpine measurement site located at the Weissfluhjoch near Davos, Switzerland, comparing the bucket scheme, Hirashima et al. (2010) scheme and the full RE, against snowpack runoff measurements from a lysimeter. The focus will be primarily on the timing and magnitude of snowpack runoff.

TCD
7, 2373–2412, 2013

2 Theory and numerical formulations

Several methods to model water flow in snow have been developed. The three that are compared here, will be discussed below.

2.1 Bucket model

In the so-called bucket model, a threshold water content (water holding capacity, θ_h) is defined, above which all the liquid water exceeding this threshold in a layer is transported downward in the snowpack or soil, regardless of the storage capacity of lower layers (Bartelt and Lehning, 2002). The downward moving water is either stored at one of the lower layers (if possible), or is drained from the model domain. In SNOWPACK, the water holding capacity varies per layer according to (Coléou and Lesaffre, 1998):

$$\theta_h = \begin{cases} 0.0264 + 0.0099\frac{(1-\theta_i)}{\theta_i}, & \theta_i \leq 0.23 \\ 0.08 - 0.1023\,(\theta_i - 0.03), & 0.23 < \theta_i \leq 0.812 \\ 0, & \theta_i > 0.812 \end{cases} \quad (1)$$

where θ_i is the volumetric ice content of the snow ($m^3\,m^{-3}$).

2.2 Richards Equation

RE describes water movement in variably saturated porous media (Richards, 1931). For a 1-dimensional column, RE can be written in a mixed-form, which can be discretized in a finite difference approximation that ensures perfect mass balance (Celia et al., 1990):

$$\frac{\partial\theta}{\partial t} - \frac{\partial}{\partial z}\left(K(\theta)\left(\frac{\partial h}{\partial z} + \cos\gamma\right)\right) + s = 0, \quad (2)$$

TCD
7, 2373–2412, 2013

where θ is the volumetric liquid water content (LWC, $m^3 m^{-3}$), K is the hydraulic conductivity ($m s^{-1}$), h is the pressure head (m), z is the vertical coordinate (positive upwards and perpendicular to the slope), γ is the slope angle and s is a source/sink term ($m^3 m^{-3} s^{-1}$).

For applying Eq. (2), a water retention curve has to be specified that relates θ to h. For snow, it is common to take the van Genuchten (1980) model:

$$\theta = \theta_r + (\theta_s - \theta_r) \frac{\left(1 + (\alpha|h|)^n\right)^{-m}}{Sc}, \quad (3)$$

where θ_r is the residual water content ($m^3 m^{-3}$), θ_s is the saturated water content ($m^3 m^{-3}$) and α is a fit coefficient that is related to the maximum pore size in the medium (m^{-1}). m and n are additional fit parameters that are related to the pore size distribution. Sc is a correction factor proposed by Ippisch et al. (2006), who have shown the necessity of using an air entry pressure when $n \leq 2$. Here, the correction is applied for all values of n, with an air entry pressure of 0.0058 m, corresponding to a largest pore size of 5 mm.

Two parameterizations for the van Genuchten (1980) model have been published recently, by Daanen and Nieber (2009) and Yamaguchi et al. (2010). By fitting to a data set from Marsh (1991), Daanen and Nieber (2009) determined the parameters α and n for the van Genuchten model to be:

$$\alpha = 30(2r_g) + 12, \quad (4)$$

and

$$n = 0.800(2r_g) + 3, \quad (5)$$

where r_g is the grain radius (mm).

TCD
7, 2373–2412, 2013

The parameterization for α proposed by Yamaguchi et al. (2010) is:

$$\alpha = 7.3(2r_g) + 1.9. \quad (6)$$

For n, the original parameterization by Yamaguchi et al. (2010) was modified by Hirashima et al. (2010) to be able to extend the parameterization beyond grain radii of 2 mm:

$$n = 15.68e^{(-0.46(2r_g))} + 1, \quad (7)$$

where for numerical stability, the upper grain radius limit is set to be 5 mm in this study.

In both parameterizations, the van Genuchten parameter m is chosen as:

$$m = 1 - (1/n), \quad (8)$$

Note that both parameterizations for the van Genuchten model for snow differ significantly. Therefore, both are taken into consideration in this study, where the Hirashima et al. (2010) modifications of the Yamaguchi et al. (2010) parameter set will be referred to as Yamaguchi and the Daanen and Nieber (2009) parameter set as Daanen.

To apply the van Genuchten model, also θ_s and θ_r need to be defined. For θ_s, it is common to take it equal to the pore space:

$$\theta_s = (1 - \theta_i)\frac{\rho_i}{\rho_w}. \quad (9)$$

Note that the correction factor at the right hand side ensures that there is enough space when liquid water freezes and thereby expands. For θ_r, Colbeck (1974) experimentally found a value of 0.07. Gravity drainage experiments by Yamaguchi et al. (2010) showed values around 0.02, suggesting that additional suction could reduce θ even more. Cold fresh snow is initially completely dry and also phase changes can reduce θ below θ_r, causing singularities in the van Genuchten model (Eq. 3) when θ is taken equal to or

TCD
7, 2373–2412, 2013

smaller than θ_r. To circumvent these problems, $\theta_r = 0$ was used and new snow layers were initialized with a very small value for θ (see Appendix A).

For determining the hydraulic conductivity, the van Genuchten–Mualem model is used (Mualem, 1976; van Genuchten, 1980):

$$K(\theta) = K_{sat}\Theta^{1/2}\left[1 - \left(1 - \Theta^{1/m}\right)^{m}\right]^{2}, \quad (10)$$

where K_{sat} is the saturated hydraulic conductivity ($m\,s^{-1}$) and Θ is the effective saturation:

$$\Theta = \frac{\theta - \theta_r}{\theta_s - \theta_r}. \quad (11)$$

K_{sat} is determined following Shimizu (1970):

$$K_{sat} = \left(\frac{\rho_w g}{\mu}\right)\left[0.077\left(\frac{r_g}{1000}\right)^{2}\exp\left(-0.0078\theta_i\rho_i\right)\right], \quad (12)$$

where ρ_w and ρ_i are respectively the density of water ($1000\,kg\,m^{-3}$) and ice ($917\,kg\,m^{-3}$), g is the gravitational acceleration (taken as $9.8\,m\,s^{-2}$) and μ is the dynamic viscosity (taken as $0.001792\,kg\,(m\,s)^{-1}$).

When snow ages, or gets involved in melt cycles, generally snow grains grow, increasing the saturated hydraulic conductivity. However, settling of the snow cover and subsequent melt cycles will increase the density, which will decrease the hydraulic conductivity. It can be easily deducted that the first effect is dominating, as grain size will generally increase by a factor 3–8, thus influencing K_{sat} by a factor 9 to 64 over a snow season. Snow density will increase by a factor 2–5, influencing K_{sat} by a factor 5 to 25 over a snow season for typical snow densities.

TCD
7, 2373–2412, 2013

2.3 NIED

Hirashima et al. (2010) developed a water transport scheme for the SNOWPACK model based on approximating the water transport by fluxes derived from Darcy's law by assuming stationary flow properties for a time step and equilibrium in water flow between two layers. RE is not explicitly solved and only downward water movement is possible. Hirashima et al. (2010) used a water retention curve based on a modified parameterization for the van Genuchten model by Yamaguchi et al. (2010). The study focussed primarily on the internal snowpack processes and achieved the reproduction of capillary barriers on the interface between layers with different grain sizes. In this study, we will refer to this water transport scheme as NIED. In Hirashima et al. (2010), θ_r was set to 0.02 but for comparison with full RE, θ_r for NIED is set to 0 as well in this study.

3 Data and methods

3.1 Data

The SNOWPACK model is forced with a meteorological data set from the experimental site at Weissfluhjoch (WFJ) at an altitude of 2540 m in the Swiss Alps near Davos. During the winter months, almost all precipitation falls as snow and as a consequence, a continuous seasonal snow cover always builds up in winter at this altitude, with a maximum snow height ranging from 140–366 cm. The measurement site is located in an almost flat part of a southeast oriented slope (γ is taken equal to 0).

The data set contains air temperature, relative humidity, wind speed and direction, incoming and outgoing longwave and shortwave radiation, surface temperature, soil temperature at a few cm below the surface, snow height and precipitation from a heated rain gauge. The data set has been quality checked, by replacing missing values with values from backup sensors or by applying various interpolation methods. The precipitation was corrected for undercatch during snowfall and windy conditions by using

TCD
7, 2373–2412, 2013

a correction proposed by Hamon (1973). Measured precipitation was assumed to be rain when the air temperature was higher than 1.2 °C and snow otherwise. For details about this data set, see Schmucki et al. (2013). The surface albedo calculated from the ratio between incoming and outgoing shortwave radiation was found to be erroneously low occasionally, resulting in excessive melt rates in spring. Therefore, simulations were driven by incoming shortwave radiation only, and using parameterized albedo to determine shortwave absorption (Groot Zwaaftink et al., 2013).

The experimental site is equipped with a lysimeter, which measures the liquid water runoff from the snowpack. The surface area of the squared lysimeter is 5 m^2 and it is measuring at a resolution of 0.8 mm. Data is collected at 10 min intervals. The lysimeter is circumvented by a barrier of 60 cm height to reduce lateral flow effects near the soil-snow interface. However, lateral flow along capillary barriers or other, more impermeable layers (e.g. melt-freeze crusts) higher in the snowpack may still affect the measurements. The lysimeter is expected to collect this meltwater advected by lateral flow mechanisms, as the device is located at the lowest part of the site.

The studied period is from 1 October 1996 to 30 September 2010. This period, consisting of 14 full winter seasons, is chosen based on data-availability and quality of the lysimeter measurements. The length of the period also ensures that some variability in meteorological conditions is present in the data set, such as several ROS events and provides the possibility to thoroughly verify the snow cover runoff as calculated by the different water transport schemes.

3.2 Methods

3.2.1 Simulation setup

The 1-dimensional mixed form of RE (Eq. 2) is solved by a Picard iteration scheme (Celia et al., 1990), adapted for a variable grid spacing based on Rathfelder and Abriola (1994). The scheme has the property of an easy numerical implementation that is

TCD
7, 2373–2412, 2013

globally convergent. In Appendix A, several aspects of the numerical implementation are discussed.

When using RE, the snowpack and the soil are considered as a single continuous column. There are no special boundary conditions for the lowest snow layer or upper-most soil layer. The snowpack runoff is calculated in a model postprocessing step by evaluating Darcy's law at the interface between the snowpack and the soil:

$$q = K\left(\frac{\partial h}{\partial z} + \cos\gamma\right) \approx K^{i+1/2}\left(\frac{h^{i+1} - h^{i}}{\Delta z} + \cos\gamma\right), \quad (13)$$

where q is the snowpack runoff ($\mathrm{m\,s^{-1}}$), positive values denoting downward water movement. The right hand side describes the numerical implementation, where i denotes the upper-most soil element and $i+1$ the lowest snow element, $K^{i+1/2}$ is the hydraulic conductivity at the interface between element i and $i+1$, and h^{i} and h^{i+1} are the pressure heads in the top soil and bottom snow element respectively. Δz is the vertical grid spacing. In the rest of the paper, snowpack runoff will be treated from a mass balance perspective, denoting downward water movement (snowpack outflow) with a negative value.

For all simulations, a soil of 1.5 m depth is used, divided into 30 layers of varying thickness. This setup ensures that choices for lower boundary conditions in the soil are only marginally impacting the snow cover. In all simulations, water flow in the soil is solved using RE. Typical soil properties for gravel/coarse sand were taken ($\theta_r = 0.01$, $\theta_s = 0.35$, $\alpha = 3.5\,\mathrm{m^{-1}}$, $n = 4.5$ and $K_{sat} = 3.171 \cdot 10^{-6}\ \mathrm{m\,s^{-1}}$). At the lower boundary, a saturated water table is prescribed as a Dirichlet boundary condition. Although in reality, the water table is expected to be deeper at WFJ, the gravel/coarse sand material will make the influence of the water table on snowpack runoff negligible small. At the lower boundary in soil, a Dirichlet boundary condition for the soil temperature of 0 °C is used.

For the snowpack, the layer thickness varies per layer and with time. When there is solid precipitation, new snow layers are added on top of the domain with an initial

TCD
7, 2373–2412, 2013

depth of 2 cm. Over time, settling of the snow reduces the layer thickness. When a snow layer gets smaller than a specified minimum height or the ice content decreases below a specified minimum value, it is joined with the layer above (in case it is the lowest snow layer) or below (all other cases). When two adjacent snow layers get similar properties, they are also joined (Bartelt and Lehning, 2002).

The model is run in 15 min time steps. Processes are described sequentially, assuming stationary snowpack behaviour in these 15 min. First, new snow is added to the snowpack at the beginning of a time step when solid precipitation is present. Then, the change in temperature distribution over the time step is calculated, after which phase changes are executed based on the new temperature profile at the end of the time step. Then the water transport routine is executed. For runs with the bucket or NIED model, first the snowpack water flow is calculated. The sum of runoff over the time step is expressed as an average runoff from the snowpack over the time step, which is then used as upper Neumann boundary condition for the RE for the soil part. For runs with RE for both snowpack and soil, the soil-snow column is calculated as a continuous column. After the calculation of water transport is finished, the new snowpack state will undergo phase change again when necessary, mainly to freeze infiltrating meltwater and rain water. The time step is finalized by calculating the internal snowpack metamorphism. Note that water transport by the NIED scheme is internally calculated with a time step of 1 min. The solver for RE uses a variable time step (see Appendix A for details).

For rain, evaporation and sublimation, heat advection by the liquid water is applied as a Neumann boundary flux for the temperature equation, while the liquid water itself is used as a specified flux (second type) boundary condition (McCord, 1991) for the water transport schemes. In the bucket and NIED simulations, the latent heat flux is first used to evaporate liquid water from the snowpack. Remaining energy was then used to sublimate the ice matrix, respecting the fact that evaporation is more favoured by the lower energy required for evaporation. When RE was used for the snowpack, the specified flux was limited. A maximum evaporative flux is allowed, based on an imaginary limiting pressure head outside the domain (see Appendix A). If the evaporative

TCD
7, 2373–2412, 2013

flux exceeds this value, the flux is limited to this value. The excess energy is used to sublimate the ice matrix.

3.2.2 Analysis

The model simulations and lysimeter measurements are analyzed for 24, 12, 6, 3, 1 and 0.5 h time scales. Runoff values were constructed by summing the 15 min model output resolution or the 10 min lysimeter measurement resolution to the respective time scales, starting at 00:00 LT (midnight local time). To determine the beginning and end of a snow season, it was assumed that on 1 March, a snow cover will always be present. Then, it was searched both forward and backward in time in the simulations until snow-free conditions were encountered in all simulations. These marked the start and end of the snow season. The winter seasons are denoted by the year in which they end (e.g., 1997 denotes winter season 1996–1997). The melt season is defined here as the period from 1 March to the melt out date. Summer snowfalls are ignored in the analysis.

In the measurements from the lysimeter, one cannot distinguish snowpack runoff with a snowpack present and rain without a snowpack. Using measured snow height to determine the end of the snow season appeared to be somewhat cumbersome as measurement inaccuracies make it difficult to determine when the surface is snow free. Moreover, the rain gauge used to derive precipitation amounts, the snow height sensor and the lysimeter are located several meters apart. Given the spatial variability of the snow cover thickness, the snow height sensor cannot be regarded as fully representative for the snow height at the lysimeter. Therefore, the runoff measured by the lysimeter was assumed to come from the snowpack as long as a snow cover was present in the simulations.

To assess the added value of the water transport schemes, the performance of modelled runoff is compared to a constructed runoff series that consists of the modelled LWC production (snow melt and rain input). This represents the case where the sum

TCD
7, 2373–2412, 2013

of snow melt and rain input is routed to runoff immediately and it will be referred to as LWC production.

To quantify the accuracy of the modelled snowpack runoff, Nash–Sutcliffe model efficiency coefficients (NSE, Nash and Sutcliffe, 1970) were calculated for all time scales. These were only determined over the winter snow season. To calculate an NSE coefficient over all 14 snow seasons, the snow seasons are analyzed sequentially by removing the intermediate summer periods.

All simulations were run on the same desktop computer as a single-core process. The simulations with the bucket scheme for snow took on average about 1.8 min per year and the NIED scheme took about 1.9 min per year. Solving RE for snow increased the average simulation time to 3.3 min per year for RE (Yamaguchi) and 2.9 min per year for RE (Daanen).

4 Results and discussion

The discussion of the results will first focus on the seasonal and daily time scale and afterwards on subdaily time scales. Table 1 shows the snow season period and the maximum snow height for each year. In the studied period, the snow season is mostly starting in October, and the melt out date is mostly between 15 June and 15 July. The maximum snow height measured with the snow height sensor ranges from 182 cm in 2005 to 356 cm in 1999. The modelled maximum snow height shows some deviation from the measured one. Differences are typically below 20 cm, although also larger deviations occur. Interestingly, the maximum snow height also varies between simulations. This is mainly caused by variation in settling of the snowpack, which is strongly dependent of the vertical distribution of LWC. As shown in Fig. 1, the cumulative runoff sum from the snowpack shows much smaller variation between the simulations, showing that there is only a small difference in modelled snow water equivalent.

We will now shortly discuss reasons for different melt curves or variations in modelled snow water equivalent, depending on the used water transport scheme. Firstly, the

TCD
7, 2373–2412, 2013

albedo of the snow cover, and thus the energy balance, is influenced by the LWC in the surface layer. Second the LWC in the surface layer will influence the variation in surface temperature, especially due to variations in time needed to refreeze at night. These differences in surface temperature in the evening hours may influence sensible and latent heat exchange and may cause differences in energy input into the snow cover between simulations. Third, the partitioning of latent heat between sublimation and evaporation is different between the water transport schemes. Because of the difference in latent heat associated with sublimation or evaporation, mass gain or loss will be smaller in case of sublimation.

Figure 1 shows that the measured runoff is generally larger than the modelled runoff, likely caused by lateral flow effects or insufficient precipitation undercatch correction. The deviations between measured and modelled runoff vary from year-to-year. Difficulties when measuring solid precipitation (Goodison et al., 1998) are one likely cause for the discrepancies between modelled and measured runoff. Furthermore, the deviations are likely a general expression of the fact that snow height can vary over short distances, mainly caused by heterogeneity in wind fields (e.g., Winstral et al., 2002; Mott et al., 2010). Only in 1997 and 2000, the deviation between measured and modelled runoff is suspiciously large. In 1997, the measured runoff is almost twice the amount of modelled runoff and in 2000, measured runoff is less then half the modelled runoff. These differences seem to be too large to be explained by lateral flow effects or inhomogeneous snow redistribution, and the agreement between measured and modelled snow height for these years (see Table 1) suggest that precipitation input is also not the cause of the differences. In both cases, the consistency between maximum measured snow height and modelled runoff indicates that the error source must be in the measured runoff due to malfunctioning of the lysimeter.

4.1 Daily time scale

For snow season 2003, all individual water transport schemes show optimal performance compared to other seasons. Therefore, this year is used as an example.

TCD
7, 2373–2412, 2013

Figure 2a shows the cumulative runoff in the melt season. As can be seen, the lysimeter registers the first melt water at the base of the snowpack much sooner than any of the model schemes. However, this involves only marginal amounts. The first important amounts of melt water arriving at the bottom of the snowpack measured by the lysimeter are reproduced well in the simulations with RE, whereas the bucket and NIED simulations show some delay. For the rest of the melt season, there are no important differences. Because the bucket and NIED simulations withhold the water too much in the snowpack compared to the lysimeter and the simulations with RE, the daily outflow in the end of the season becomes higher than in simulations with RE. Figure 3a shows the NSE coefficients for daily sums of runoff for the 14 yr individually. It shows that for the daily time scale, differences between the various models are much smaller than year-to-year differences in NSE coefficients. However, this is mainly dominated by three years with NSE coefficients lower than 0.4. Typical causes for low NSE values are a consistent over or underestimation (bias) and poor timing of meltwater peaks (McCuen et al., 2006). For the years 1997 and 2000, the low NSE coefficients are for an important part caused by the bias between modelled and measured seasonal runoff (see Fig. 1). For the year 2005, it appears as if the lysimeter was obstructed for quite some time, after which half the seasonal sum of runoff passed through the device in a few days time (not shown).

For the other years, Fig. 3a shows that when the agreement between modelled and measured runoff is lower, all water transport schemes have a lower agreement and vice versa. The fact that NSE coefficients for LWC production follow the same pattern is an indication that for these years, sources of error causing variation of NSE coefficients may be related to the estimation of meltwater production as determined by a positive energy balance and a possibly sometimes inaccurate partitioning of precipitation in rain and snow. The representation of internal snowpack structure and accompanying hydraulic properties in the model seem to play a less pronounced role.

On the other hand, lysimeter measurements are known to be notoriously difficult, as found in experiments by Kattelmann (2000). Discrepancies between measured and

TCD
7, 2373–2412, 2013

modelled runoff should therefore not be attributed solely to an inaccurate representation of the snow cover or energy balance in the model. For example, the fences around the lysimeter to prevent preferential flow along the base of the snowpack may influence the snow cover at the start of the snow season. The lysimeter may collect more snow due to wind effects and snowmelt can be reduced due to the shadowing effect of the fence. This may lead to a non-representative snow cover inside the lysimeter.

Over all 14 seasons, using RE does reproduce measured runoff best, with both Yamaguchi and Daanen parameterizations giving a NSE coefficient of 0.60. Bucket and NIED also have very similar performance with NSE coefficients of 0.56 and 0.58 respectively. The fact that the different water transport schemes have very similar performance on the daily time scale and have an NSE coefficient very similar to the one for LWC production is indicating that once the snowpack is isothermal, meltwater produced near the surface is transported downward within the day in all models and that this is in good agreement with the measurements. This is noted already in literature (e.g., Colbeck, 1972; Davis et al., 2001).

4.2 Timing of seasonal runoff

To assess the model performance in simulating the timing of the runoff throughout the melt season (starting 1 March), it was determined at which date a certain percentage of the total cumulative snowpack runoff was reached. This was also done for the measurements. Then the difference between measured and modelled date was determined. Figure 4 shows the time delay in days between modelled and measured runoff. A positive delay means that modelled cumulative runoff is achieved later in time than the measured one. For example: 20 % of total runoff is delayed by 2 days in the RE (Yamaguchi) simulations and 5 days in the bucket simulations.

As can be seen, all models are strongly underestimating the arrival date of the first few percent of the total runoff, up to about 20 days for the bucket and NIED scheme. However, LWC production in the model is also lagging behind measured runoff, suggesting that the water in the first measured runoff does not originate from the snow

TCD
7, 2373–2412, 2013

cover above the lysimeter, but is advected by lateral flow from parts of the slope that receives more shortwave radiation.

The RE (Yamaguchi) simulations quickly come into the range of the measured runoff. For values of about 5 % and above, the runoff is delayed by 2–3 days. RE (Daanen) is slightly lagging RE (Yamaguchi). The bucket and NIED model have a delayed runoff much longer and only after about 40 – 50 % of runoff has occurred, the remaining delay time is more or less similar to the RE simulations (about 2–3 days). Apparently, bucket and NIED are retaining meltwater in the snowpack too long, releasing it later in the melt season. Except for the approximately first 5 % of runoff, RE simulations are much closer to the measured runoff. The fact that the delay is fairly constant after about 15 % shows that the daily amount of meltwater leaving the snowpack is in quite good agreement with measured values.

Apart from lateral flow, the fast arrival of meltwater at the base of the snowpack in the measurements may also result from the more efficient transport mechanism of preferential flow paths compared to matrix flow. Several experiments have shown that water flow in snow is not horizontally homogeneous (e.g., Conway and Benedict, 1994; Waldner et al., 2004; Katsushima et al., 2013). The 1-D approach in this study cannot resolve preferential flow paths by flow fingering, as observed in several experiments. Preferential flow paths will be able to transport water downward faster than horizontally uniform matrix flow, as simulated in the 1-D SNOWPACK model. However, Fig. 4 suggest that this may involve about 5 % of cumulative seasonal runoff. Note that this does certainly not imply that preferential flow cannot have a more pronounced effect on the internal snowpack microstructure or wet snow avalanche formation.

4.3 Sub-daily time scales

Figure 2b shows the hourly flux of snowpack runoff for one week during the melt season of the example snow season 2003. A daily returning peak in melt water outflow, associated with the daily cycle in melt, is visible. The timing of the peak flux is better reproduced by simulations with RE. The figure also shows that RE is able to reproduce

TCD
7, 2373–2412, 2013

the recession curve in the evening hours and the night. Although in this figure, the NIED model does not reproduce this recession curve for the WFJ, Hirashima et al. (2013) recently found that the recession curve is also reproduced in the NIED scheme for warm snow regions such as the central part of Japan.

In Fig. 5, NSE coefficients for the various water transport schemes are shown for sub-daily time scales. The water transport schemes produce more or less similar results on the 12 and 24 h time scale, with the RE using the Yamaguchi parameterization performing best in terms of NSE. For smaller time scales, the NSE coefficients are decreasing, especially for the bucket and NIED simulations. For the 1 h time scale, RE (Yamaguchi) achieves a still reasonable NSE coefficient of 0.48, where bucket and NIED have NSE coefficients of 0.16 and −0.05 respectively. Also the constructed runoff series from LWC production shows a strong decrease in NSE coefficient on the smaller time scales, indicating the importance of travel time and intermediate storage in the snow cover. The decrease in NSE coefficient for the bucket and NIED simulations must be mainly caused by poor timing of the meltwater release by these schemes, as the daily sums of modelled runoff do not show large differences (see Fig. 3a).

Figure 3b shows that the NSE coefficients for 1 h sums of runoff exhibit variation from year-to-year. For bucket and NIED simulations, NSE coefficients for hourly runoff are close to zero or even negative, indicating that the model has poor performance on the hourly time scale. RE shows a much better agreement with measurements than the other two models for most years, with Yamaguchi's parameterization being the best.

4.4 Timing of hourly runoff

The NSE coefficients for the hourly time scale were close to 0 or even negative for the bucket and NIED model, which was ascribed to poor timing of the meltwater release in the bucket and NIED simulations. To quantify the timing of runoff, lag correlations were calculated between each of the simulations and the measured runoff. The time span was limited to −12 and +12 h, to prevent correlations with the daily cycle. Table 2 shows the time lag belonging to the highest lag correlation, with negative values indicating the

TCD
7, 2373–2412, 2013

runoff is too early in the day in the simulations. As can be seen, the bucket and NIED model have about 1–2 h too early runoff compared to measured runoff, while both simulations with RE show fairly good agreement in timing. Yamaguchi's parameterization seems to provide the best agreement with the measurements. The time lag between LWC production and measured runoff is about 1–3 h, showing the effect of the travel time through the snow cover for the sub-daily time scale.

The simulations with RE did not show an important time lag between lysimeter measurements and modelled runoff. The existence of preferential flow paths in snow with a more efficient water transport mechanism compared to matrix flow would give the expectation that a time lag would exist. Three issues may play a role here. Firstly, it may be that the existence of preferential flow paths is not essential for correctly modelling snowpack runoff, because the amount of water involved in preferential flow is small. Second, it is possible that the experiments to derive parameterizations for the hydraulic conductivity already incorporate preferential flow effects due to the measurement setup in which average flow behaviour is observed. Third, the choice of $\theta_r = 0$ results in direct participation of all liquid water in water transport. This may be a simplification of reality that would compensate for the error of neglecting preferential flow paths in the model.

4.5 Relation modelled and measured runoff

Figures 6 and 7 show scatter density plots for both the bucket model and RE (Yamaguchi) model for both the 24 h and 1 h time scale. In these figures, the years 1997, 2000 and 2005 are left out, as the high discrepancy between modelled and measured runoff for these years, suggesting measurement problems as discussed before, can beforehand be expected to cause a bias in these figures. The figures show the relative distribution of combinations of measured and modelled snowpack runoff for the 11 remaining snow seasons.

For the 24 h time scale, the scatter density plots for both water transport models look very similar, in contrast to the 1 h time scale. Combined with an almost equal r^2

TCD
7, 2373–2412, 2013

value, this confirms the conclusion that all water transport schemes have almost equal performance on the daily time scale.

The distribution for the 1 h time scale shows that with RE (Yamaguchi), modelled runoff agrees better with measured runoff. This is also expressed by the much higher r^2 value. Besides this main distribution along the diagonal where modelled runoff equals measured runoff, two distinct features are found. First, the bucket model seems to produce considerable amounts of runoff (−2 to −5 mm h^{-1}) when there is almost no runoff measured. This effect was not present on the 24 hour time scale, so it likely originates from the fact that the bucket model is bringing meltwater down too quickly on the hourly time scale (see Table 2). Secondly, especially in the RE (Yamaguchi) model, there is snowpack runoff observed in the order of −2 to −4 mm h^{-1}, where at the same time the modelled runoff is close to zero.

5 Conclusions

A comparison of measured snowpack runoff by a lysimeter and 3 water transport schemes for a physical based snowpack model has shown that simulating water flow through a snow cover using RE achieves the best agreement with a modest increase in computation effort. NSE coefficients and r^2 values for simulations with RE were higher on both the daily and sub-daily time scales when compared to bucket and NIED simulations. The strongest improvement is on the sub-daily time scales. The NSE coefficients vary from year-to-year, quite synchronously: years with lower NSE coefficients have low NSE coefficients in all water transport schemes and vice versa. This indicates that measurements of either runoff or meteorological forcing have systematic errors that also vary from year to year.

The timing of meltwater arrival at the base of the snowpack also improved with RE, for both the daily and the sub-daily time scale. On the seasonal time scale, bucket and NIED simulations seem to retain the meltwater in the snowpack too long, underestimating the arrival of meltwater at the base of the snowpack in the early stages of the

TCD
7, 2373–2412, 2013

melt season. The results confirm that after the snow cover has become isothermal, the runoff is mainly determined by the meltwater production near the surface due to a positive energy balance and all water transport schemes route this water to runoff within the day, causing similar performance on the daily time scale.

For the sub-daily time scale, lag correlation coefficients showed that bucket and NIED simulations release meltwater too early in the day compared to measured runoff. This is mainly because the water transport schemes in these two simulations do not incorporate or underestimate travel time of liquid water through the snowpack. For RE, the timing of both seasonal and daily runoff is in better agreement with measured runoff. Of the two parameterizations of the water retention curve in the van Genuchten model, Yamaguchi's parameterization has on average the best representation of travel time, whereas Daanen's parameterization causes a little too slow travel time.

This study has shown that solving RE for snow is improving several aspects of modelled snowpack runoff considerably. Yamaguchi's parameterization shows the best overall performance, especially in terms of NSE coefficients. The LWC distribution in the snowpack when using Daanen's parameterization seems to cause much slower settling in SNOWPACK, overestimating snow heights. This will be a drawback in some applications, especially if snow depth is used to calculate winter precipitation (Lehning et al., 2002a). Note that this study did not consider the internal snowpack microstructure or the LWC or density distribution but focussed only on snowpack runoff. The use of RE may have a considerable effect on these internal snowpack properties. For example, the assumption of $\theta_r = 0$ may lead to an underestimation of melt metamorphism.

6 Outlook

As was pointed out by Marsh (1999), there is a strong need for a better understanding and improved models to describe the complex water flow in natural snow covers. This study has shown that when only looking at snowpack runoff, improving water transport models has an important consequence for the accuracy of snowpack runoff modelling.

TCD
7, 2373–2412, 2013

Because the number of experimental studies analyzing liquid water flow in snow is limited, the results in this study suggest that more experiments for different snow types are welcome as there is potential for the improvement of the model performance of water flow in snow. Moreover, the improvement in performance regarding snowpack runoff suggests that a deeper analysis on the effects on the internal microstructure of the snow, such as the formation of melt-freeze crusts is needed.

Appendix

Solving RE for snow involves some numerical challenges. Generally, many layers will form in a simulation with a considerable snowpack such as at Weissfluhjoch. These layers can cause strong inhomogeneities in grain size and density, impacting numerical performance. Here, the specific numerical implementation will be discussed with some best practice methodology.

A1 Time step control

To be able to simulate a complete snow season with optimal numerical performance, it is unavoidable to use variable time steps, as the dry snowpack in the winter months can be treated with much larger time steps than the spring snow melt or ROS events. Infiltration fronts of meltwater in dry snow or soil require small time steps, because Picard iteration is known to have slow convergence for these situations (Paniconi and Putti, 1994). We apply the time stepping approach proposed by Paniconi and Putti (1994). Based on the number of iterations needed for convergence in the Picard scheme (N_{iter}), the new time step Δt_{new} is based on the previous time step Δt_{old} according to (deter-

TCD
7, 2373–2412, 2013

mined by trial and error):

$$\Delta t_{\text{new}} = \begin{cases} 1.25\Delta t_{\text{old}}, & N_{\text{iter}} \leq 5 \\ \Delta t_{\text{old}}, & 5 < N_{\text{iter}} \leq 10 \\ 0.5\Delta t_{\text{old}}, & 10 < N_{\text{iter}} \leq 15 \\ \text{back-step}, & N_{\text{iter}} > 15 \end{cases} \quad \text{(A1)}$$

When a back-step is performed, the time step is repeated with a smaller time step: $\Delta t_{\text{new}} = f_{\text{bs}} \Delta t_{\text{old}}$, with $f_{\text{bs}} = (1/3)^{n_{\text{sb}}}$ and n_{sb} being the number of sequential back-steps (for 1st backstep: $n_{\text{sb}} = 1$). Back steps are not only performed when $N_{\text{iter}} > 15$, but also when (i) change in pressure head between iterations exceeds a prescribed value (10^3 m) or (ii) the mass balance is strongly violated (mass balance error > 0.1 kg m^{-2}). Both are early signs of growing model instabilities due to a too large time step. Doing a backstep immediately saves computation time by not executing all 15 iterations.

A2 Convergence criterion

To determine convergence of the solution, the absolute change in solution between two iterations is required to be below a certain threshold. In the proposed Picard iteration by Celia et al. (1990), convergence is checked by a threshold value for the change in pressure head ($\Delta h < \epsilon_h$). However, Huang et al. (1996) have found that for non near-saturated conditions, determining convergence based on a threshold for θ ($\Delta\theta < \epsilon_\theta$) will also work and will generally improve convergence considerably, especially in dry conditions as often found in the snowpack. However, close to saturation and in ponding conditions, determining convergence based on θ will not work and the pressure head criterion should be used. Therefore, it is set that where $\theta > 0.99$, the pressure head criterion is used and the θ criterion elsewhere. The θ criterion at low saturation can cause very inaccurate pressure head estimations and consequently large errors in the flux determined by Eq. (13). To achieve an accurate estimation of the snow-soil interface flux, convergence in the upper-most soil layer and lowest snow layer is always

TCD
7, 2373–2412, 2013

judged by the pressure head criterion. Values for ϵ_h and ϵ_θ are set to $1 \cdot 10^{-3}$ m and $1 \cdot 10^{-5}$ m^3 m^{-3} respectively, based on Huang et al. (1996).

A3 Treatment of dry snow layers

Fresh snow is dry below freezing. This gives a singularity in the Van Genuchten model for $\theta = \theta_r$, associated with an infinitely low pressure head. This singularity is circumvented by initializing these new dry snow layers with a very low pressure head. The following algorithm was used to determine the initial pressure head for dry snow layers: for each layer, the pressure head associated with $\theta = \theta_r + \frac{\epsilon_\theta}{10}$ was determined, so not detectable by the convergence criterion. The smallest value found for pressure head was chosen to initialize dry snow layers with. The associated tiny amount of LWC was created by melting the ice matrix. To prevent a continuously refreezing and subsequent melting of these tiny amounts of water in the snow cover, refreezing of meltwater in snow was only allowed for LWC exceeding 0.01 %. This value is small enough not to influence other snowpack calculations (e.g., wet snow metamorphism). The initialization value of the pressure head was also used to determine the maximum allowed evaporative flux at the top of the domain, by prescribing it for an imaginary grid point outside the model domain.

A4 Hydraulic conductivity at the interface between nodes

The finite difference approach to solve RE uses the center point of snowpack layers as nodes. The scheme therefore requires an estimation of the hydraulic conductivity at the interface between two layers. In literature, several methods to approximate hydraulic conductivity at the interface nodes between layers have been proposed (e.g., harmonic averaging, geometric averaging, see for example Szymkiewicz and Helmig, 2011). Several approaches were tested, but many yield very bad numerical performance and many tests would not complete within reasonable time. Main problems arise at interfaces where the hydraulic conductivity varies over several orders of magnitude

TCD
7, 2373–2412, 2013

(dry fresh snow layers on top of old snowpack). Most proposed averaging methods tend to put more weight on the lowest value for K. Arithmetic mean was found to work best, as it will effectively smooth large gradients in hydraulic conductivity. We suggest that the limited knowledge of hydraulic properties of snow is likely to more strongly influence calculation results than errors arising from inaccurate approximations of the hydraulic conductivity at the interface nodes.

Acknowledgements. This research has been conducted in the framework of the IRKIS project supported by the Office for Forests and Natural Hazards of the Swiss Canton of Grisons (Chr. Wilhelm), the region of South Tyrol (Italy) and the community of Davos. General infrastructure support from N. Dawes and M. Ruesch is acknowledged.

References

Bartelt, P. and Lehning, M.: A physical SNOWPACK model for the Swiss avalanche warning – Part I: numerical model, Cold Reg. Sci. Technol., 35, 123–145, doi:10.1016/S0165-232X(02)00074-5, 2002. 2376, 2377, 2384

Boone, A. and Etchevers, P.: An intercomparison of three snow schemes of varying complexity coupled to the same land surface model: local-scale evaluation at an Alpine site, J. Hydrometeor., 2, 374–394, doi:10.1175/1525-7541(2001)002<0374:AIOTSS>2.0.CO;2, 2001. 2375

Brun, E., Martin, E., Simon, V., Gendre, C., and Coléou, C.: An energy and mass model of snow cover suitable for operational avalanche forecasting, J. Glaciol., 35, 333–342, 1989. 2376

Celia, M. A., Bouloutas, E. T., and Zarba, R. L.: A general mass-conservative numerical solution for the unsaturated flow equation, Water Resour. Res., 26, 1483–1496, doi:10.1029/WR026i007p01483, 1990. 2377, 2382, 2396

Colbeck, S. C.: A theory of water percolation in snow, J. Glaciol., 11, 369–385, 1972. 2376, 2389

Colbeck, S. C.: The capillary effects on water percolation in homogeneous snow, J. Glaciol., 13, 85–97, 1974. 2375, 2376, 2379

Coléou, C. and Lesaffre, B.: Irreducible water saturation in snow: experimental results in a cold laboratory, Ann. Glaciol., 26, 64–68, 1998. 2377

TCD
7, 2373–2412, 2013

Conway, H. and Benedict, R.: Infiltration of water into snow, Water Resour. Res., 30, 641–649, doi:10.1029/93WR03247, 1994. 2390
Conway, H. and Raymond, C. F.: Snow stability during rain, J. Glaciol., 39, 635–642, 1993. 2375
Daanen, R. and Nieber, J.: Model for coupled liquid water flow and heat transport with phase change in a snowpack, J. Cold Reg. Eng., 23, 43–68, doi:10.1061/(ASCE)0887-381X(2009)23:2(43), 2009. 2376, 2378, 2379
Davis, R. E., Jordan, R., Daly, S., and Koenig, G. G.: Model Validation: Perspectives in Hydrological Science, John Wiley & Sons Ltd, 2001. 2376, 2389
Goodison, B., Louie, P., and Yang, D.: WMO Solid precipitation measurement intercomparison, Final Report, Tech. rep., World Meteorological Organization (WMO), 1998. 2387
Groot Zwaaftink, C. D., Cagnati, A., Crepaz, A., Fierz, C., Macelloni, G., Valt, M., and Lehning, M.: Event-driven deposition of snow on the Antarctic Plateau: analyzing field measurements with SNOWPACK, The Cryosphere, 7, 333–347, doi:10.5194/tc-7-333-2013, 2013. 2382
Hamon, W.: Computing actual precipitation, in: Proceedings of WMO-IAHS: Symposium on the Distribution of Precipitation in Mountainous Areas, vol. 1, pp. 159–173, World Meteorological Organization, 1973. 2382
Hirashima, H., Yamaguchi, S., Sato, A., and Lehning, M.: Numerical modeling of liquid water movement through layered snow based on new measurements of the water retention curve, Cold Reg. Sci. Technol., 64, 94–103, doi:10.1016/j.coldregions.2010.09.003, 2010. 2376, 2379, 2381
Hirashima, H., Satoru, Y., Kamiishi, I., Sato, A., and Lehning, M.: Numerical modeling of liquid water movement in snowpack: arrival at the snow base and subsequent infiltration into the substrate, Cold Reg. Sci. Technol., in review, 2013. 2391
Huang, K., Mohanty, B., and van Genuchten, M.: A new convergence criterion for the modified Picard iteration method to solve the variably saturated flow equation, J. Hydrol., 178, 69–91, doi:10.1016/0022-1694(95)02799-8, 1996. 2396, 2397
Illangasekare, T. H., Walter Jr., R. J., Meier, M. F., and Pfeffer, W. T.: Modeling of meltwater infiltration in subfreezing snow, Water Resour. Res., 26, 1001–1012, doi:10.1029/WR026i005p01001, 1990. 2376

TCD
7, 2373–2412, 2013

Ippisch, O., Vogel, H.-J., and Bastian, P.: Validity limits for the van Genuchten–Mualem model and implications for parameter estimation and numerical simulation, Adv. Water Res., 29, 1780–1789, doi:10.1016/j.advwatres.2005.12.011, 2006. 2378

Jin, J., Gao, X., Yang, Z.-L., Bales, R. C., Sorooshian, S., Dickinson, R. E., Sun, S. F., and Wu, G. X.: Comparative analyses of physically based snowmelt models for climate simulations, J. Climate, 12, 2643–2657, doi:10.1175/1520-0442(1999)012<2643:CAOPBS>2.0.CO;2, 1999. 2375

Jordan, P.: Meltwater movement in a deep snowpack: 2. Simulation model, Water Resour. Res., 19, 979–985, doi:10.1029/WR019i004p00979, 1983. 2376

Jordan, R.: A one-dimensional temperature model for a snow cover: technical documentation: technical documentation SNTHERM.89, Tech. Rep. Spec. Rep. 657, US Army Cold Reg. Res. Eng. Lab., Hanover, N. H., 1991. 2376

Jordan, R.: Effects of capillary discontinuities on water flow and water retention in layered snowcovers, in: Proceedings of the International Symposium on Snow and Related Manifestations, edited by: Agrawal, K. C., Snow and Avalanche Study Establishment, vol. 94, 157–170, Manali, India, 1996. 2375, 2376

Katsushima, T., Yamaguchi, S., Kumakura, T., and Sato, A.: Experimental analysis of preferential flow in dry snowpack, Cold Reg. Sci. Technol., 85, 206–216, doi:10.1016/j.coldregions.2012.09.012, 2013. 2375, 2390

Kattelmann, R.: Macropores in snowpacks of Sierra Nevada, Ann. Glaciol., 6, 272–273, 1985. 2375

Kattelmann, R.: Snowmelt lysimeters in the evaluation of snowmelt models, Ann. Glaciol., 31, 406–410, doi:10.3189/172756400781820048, 2000. 2388

Koster, R. D., Mahanama, S. P. P., Livneh, B., Lettenmaier, D. P., and Reichle, R. H.: Skill in streamflow forecasts derived from large-scale estimates of soil moisture and snow, Nature Geosci., 3, 613–616, doi:10.1038/ngeo944, 2010. 2374

Lehning, M., Bartelt, P., Brown, B., and Fierz, C.: A physical SNOWPACK model for the Swiss avalanche warning – Part III: meteorological forcing, thin layer formation and evaluation, Cold Reg. Sci. Technol., 35, 169–184, doi:10.1016/S0165-232X(02)00072-1, 2002a. 2376, 2394

Lehning, M., Bartelt, P., Brown, B., Fierz, C., and Satyawali, P.: A physical SNOWPACK model for the Swiss avalanche warning – Part II: snow microstructure, Cold Reg. Sci. Technol., 35, 147–167, doi:10.1016/S0165-232X(02)00073-3, 2002b. 2376

TCD
7, 2373–2412, 2013

Mahanama, S. P., Livneh, B., Koster, R., Lettenmaier, D., and Reichle, R.: Soil moisture, snow, and seasonal streamflow forecasts in the US, J. Hydrometeor., 13, 189–203, doi:10.1175/JHM-D-11-046.1, 2012. 2374

Marks, D., Domingo, J., Susong, D., Link, T., and Garen, D.: A spatially distributed energy balance snowmelt model for application in mountain basins, Hydrol. Proc., 13, 1935–1959, doi:10.1002/(SICI)1099-1085(199909)13:12/13<1935::AID-HYP868>3.0.CO;2-C, 1999. 2375

Marks, D., Link, T., Winstral, A., and Garen, D.: Simulating snowmelt processes during rain-on-snow over a semi-arid mountain basin, Ann. Glaciol., 32, 195–202, doi:10.3189/172756401781819751, 2001. 2375

Marsh, P.: Water flux in melting snow covers, vol. 1 of Advances in Porous Media, Elsevier, Amsterdam, 61–124, 1991. 2375, 2376, 2378

Marsh, P.: Snowcover formation and melt: recent advances and future prospects, Hydrol. Proc., 13, 2117–2134, doi:10.1002/(SICI)1099-1085(199910)13:14/15<2117::AID-HYP869>3.0.CO;2-9, 1999. 2394

Mazurkiewicz, A. B., Callery, D. G., and McDonnell, J. J.: Assessing the controls of the snow energy balance and water available for runoff in a rain-on-snow environment, J. Hydrol., 354, 1–14, doi:10.1016/j.jhydrol.2007.12.027, 2008. 2375

McCord, J. T.: Application of second-type boundaries in unsaturated flow modeling, Water Resour. Res., 27, 3257–3260, doi:10.1029/91WR02158, 1991. 2384

McCuen, R., Knight, Z., and Cutter, A.: Evaluation of the Nash–Sutcliffe Efficiency Index, J. Hydrol. Eng., 11, 597–602, doi:10.1061/(ASCE)1084-0699(2006)11:6(597), 2006. 2388

Mitterer, C., Hirashima, H., and Schweizer, J.: Wet-snow instabilities: comparison of measured and modelled liquid water content and snow stratigraphy, Ann. Glaciol., 52, 201–208, doi:10.3189/172756411797252077, 2011. 2375

Mott, R., Schirmer, M., Bavay, M., Grünewald, T., and Lehning, M.: Understanding snow-transport processes shaping the mountain snow-cover, The Cryosphere, 4, 545–559, doi:10.5194/tc-4-545-2010, 2010. 2387

Mualem, Y.: A new model for predicting the hydraulic conductivity of unsaturated porous media, Water Resour. Res., 12, 513–522, doi:10.1029/WR012i003p00513, 1976. 2380

Nash, J. and Sutcliffe, J.: River flow forecasting through conceptual models part I – a discussion of principles, J. Hydrol., 10, 282–290, doi:10.1016/0022-1694(70)90255-6, 1970. 2386

TCD
7, 2373–2412, 2013

Paniconi, C. and Putti, M.: A comparison of Picard and Newton iteration in the numerical solution of multidimensional variably saturated flow problems, Water Resour. Res., 30, 3357–3374, doi:10.1029/94WR02046, 1994. 2395
Peitzsch, E., Karl, B., and Kathy., H.: Water movement and capillary barriers in a stratified and inclined snowpack, in: Proceedings Whistler 2008 International Snow Science Workshop, September 21–27, 179–187, 2008. 2375
Rathfelder, K. and Abriola, L. M.: Mass conservative numerical solutions of the head-based Richards equation, Water Resour. Res., 30, 2579–2586, doi:10.1029/94WR01302, 1994. 2382
Richards, L.: Capillary conduction of liquids through porous mediums, J. Appl. Phys., 1, 318–333, doi:10.1063/1.1745010, 1931. 2376, 2377
Schmucki, E., Marty, C., Fierz, C., and Lehning, M.: How to run detailed energy balance snow models from weather station observations, Cold Reg. Sci. Technol., in review, 2013. 2382
Schneebeli, M.: Development and stability of preferential flow paths in a layered snowpack, in: Biogeochemistry of Seasonally Snow–Covered Catchments (Proceedings of a Boulder Symposium July 1995), edited by: Tonnessen, K., Williams, M., and Tranter, M., AHS Publ. no. 228, 89–95, 1995. 2375
Seyfried, M. S., Grant, L. E., Marks, D., Winstral, A., and McNamara, J.: Simulated soil water storage effects on streamflow generation in a mountainous snowmelt environment, Idaho, USA, Hydrol. Proc., 23, 858–873, doi:10.1002/hyp.7211, 2009. 2374
Shimizu, H.: Air permeability of deposited snow, Institute of Low Temperature Science, Sapporo, Japan, 1970. 2375, 2376, 2380
Szymkiewicz, A. and Helmig, R.: Comparison of conductivity averaging methods for one-dimensional unsaturated flow in layered soils, Adv. Water Res., 34, 1012–1025, doi:10.1016/j.advwatres.2011.05.011, 2011. 2397
van Genuchten, M. T.: A closed-form equation for predicting the hydraulic conductivity of unsaturated soils, Soil Sci. Soc. Am. J., 44, 892–898, doi:10.2136/sssaj1980.03615995004400050002x, 1980. 2378, 2380
Waldner, P. A., Schneebeli, M., Schultze-Zimmermann, U., and Flühler, H.: Effect of snow structure on water flow and solute transport, Hydrol. Proc., 18, 1271–1290, doi:10.1002/hyp.1401, 2004. 2375, 2390

TCD
7, 2373–2412, 2013

Winstral, A., Elder, K., and Davis, R. E.: Spatial snow modeling of wind-redistributed snow using terrain-based parameters, J. Hydrometeor., 3, 524–538, doi:10.1175/1525-7541(2002)003<0524:SSMOWR>2.0.CO;2, 2002. 2387

Yamaguchi, S., Katsushima, T., Sato, A., and Kumakura, T.: Water retention curve of snow with different grain sizes, Cold Reg. Sci. Technol., 64, 87–93, doi:10.1016/j.coldregions.2010.05.008, 2010. 2375, 2376, 2378, 2379, 2381

Zanotti, F., Endrizzi, S., Bertoldi, G., and Rigon, R.: The GEOTOP snow module, Hydrol. Proc., 18, 3667–3679, doi:10.1002/hyp.5794, 2004. 2375

TCD
7, 2373–2412, 2013

Table 1. Duration and maximum snow height for the 14 snow seasons.

Snow season	Duration	Maximum snow height (cm)				
		Measured	Bucket	NIED	RE (Yamaguchi)	RE (Daanen)
1997	01-10–16-07	257	241	240	237	254
1998	09-10–29-06	203	181	180	192	195
1999	11-09–01-08	356	377	375	380	408
2000	25-09–04-07	288	304	303	314	333
2001	30-10–09-07	289	243	243	254	261
2002	30-08–25-06	225	246	243	233	251
2003	21-09–16-06	245	235	235	241	257
2004	03-10–26-07	262	276	276	281	306
2005	04-11–25-06	182	188	188	192	210
2006	28-09–27-06	207	193	188	191	201
2007	31-10–11-06	190	162	162	173	178
2008	02-09–28-06	288	249	248	254	264
2009	12-09–30-06	267	247	246	251	268
2010	09-10–03-07	217	196	198	204	211

TCD
7, 2373–2412, 2013

Table 2. Lag correlation coefficients (hours) for modelled runoff compared to measured runoff. Negative values mean the measured runoff should be shifted back in time to match modelled runoff.

Snow season	Lag correlation with measured runoff (hours)				
	Bucket	NIED	RE (Yamaguchi)	RE (Daanen)	LWC production
1997	−1	−1	0.5	1	−2.5
1998	−1	−1	0	1	−1
1999	−0.5	−0.5	0.5	2.5	−0.5
2000	−3.5	−4	1.5	3	−3
2001	−1.5	−1.5	0	0	−1.5
2002	0	−0.5	0	0.5	−0.5
2003	−0.5	−0.5	0	0	−0.5
2004	−0.5	−0.5	1	3	−2
2005	−1	−1.5	0	0.5	−1.5
2006	−1	−1	0	1	−1
2007	−1.5	−1.5	0	0	−3.5
2008	−2	−2	0	0.5	−2.5
2009	−2.5	−2.5	0	0	−3
2010	−1	−1	0	0.5	−1.5

TCD
7, 2373–2412, 2013

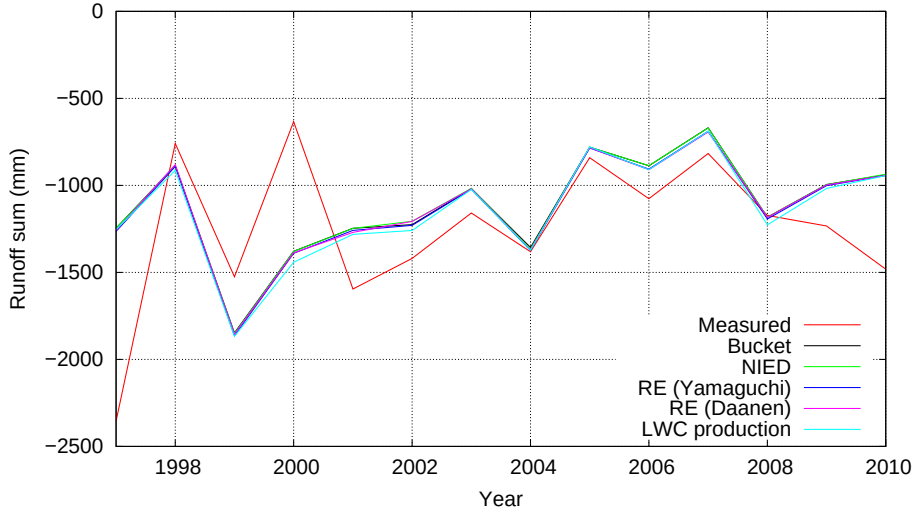

Fig. 1. Measured and modelled runoff sums over the snow seasons (mm).

TCD
7, 2373–2412, 2013

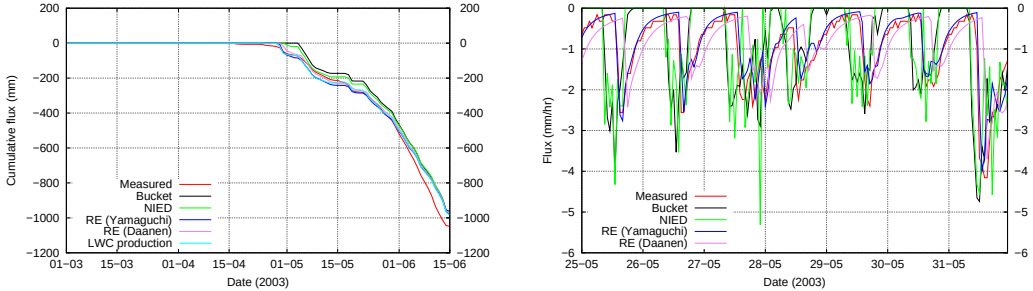

Fig. 2. Cumulative snowpack runoff for the lysimeter measurements and the various water transport schemes for the 2003 melt season **(a)** and hourly snowpack runoff for the lysimeter measurements and the various water transport schemes for one week during the 2003 melt season **(b)**.

TCD
7, 2373–2412, 2013

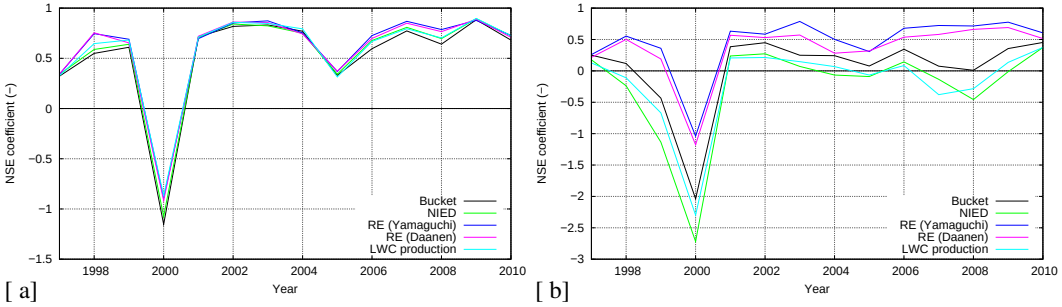

Fig. 3. NSE coefficients for the snow seasons for the 24 h time scale **(a)** and the 1 h time scale **(b)**.

TCD
7, 2373–2412, 2013

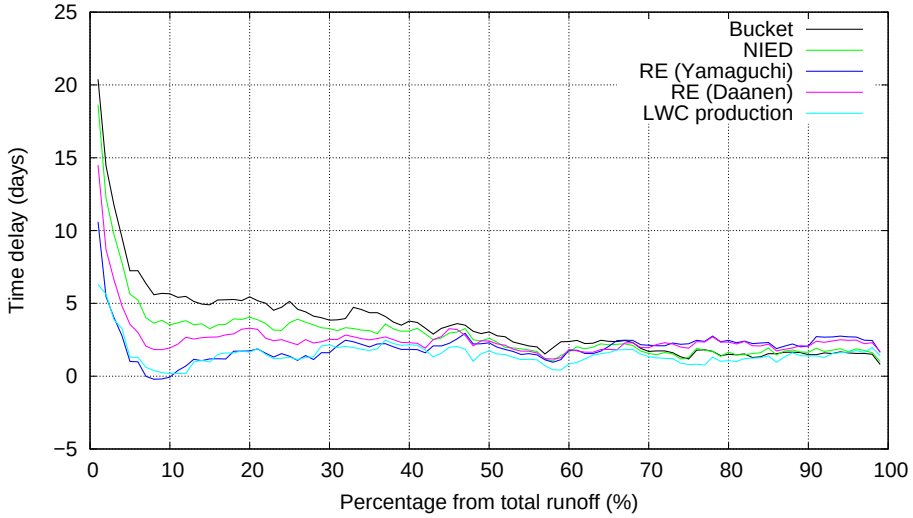

Fig. 4. Delay between modelled and observed runoff as a function of percentage of total melt season runoff (starting 1 March).

TCD
7, 2373–2412, 2013

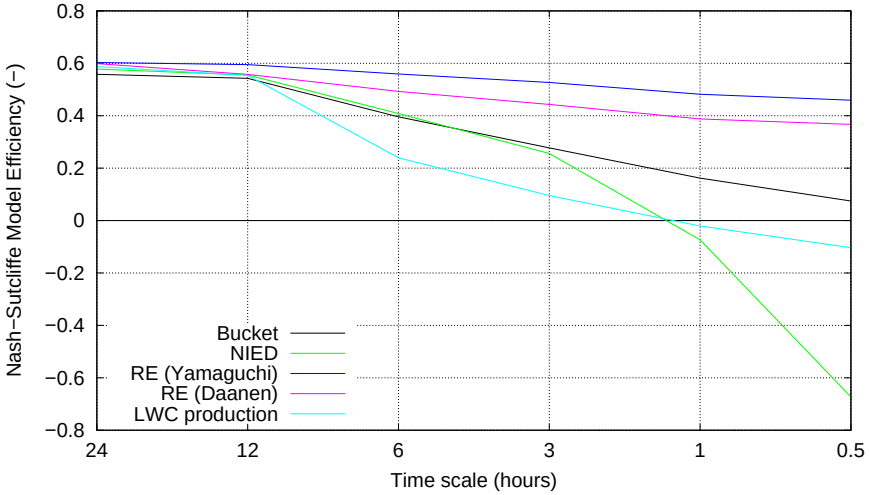

Fig. 5. NSE coefficients over all snow seasons for the studied water transport algorithms for different time scales.

TCD
7, 2373–2412, 2013

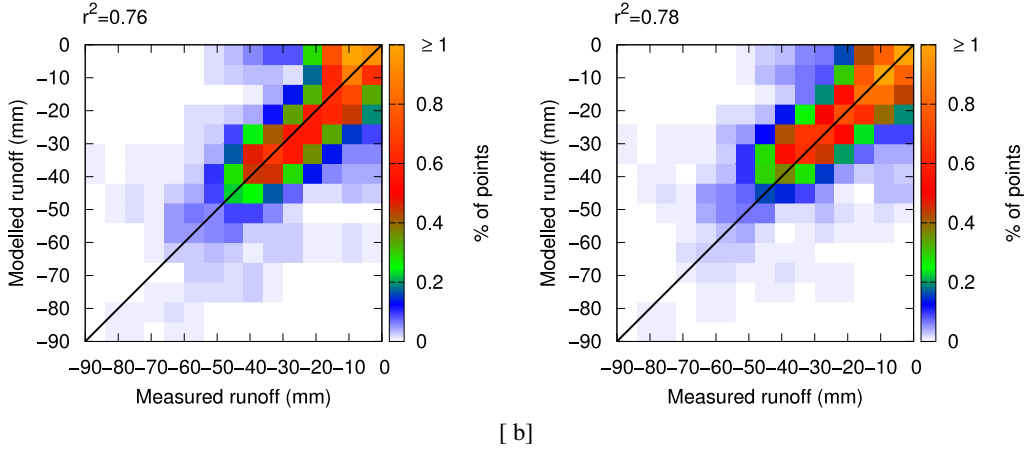

Fig. 6. Density scatter plots for modelled versus measured runoff (mm) for the 24 hour time scale for the bucket model **(a)** and RE (Yamaguchi) model **(b)**. In colour are shown the percentages in the specific region, cut off at 1 %.

TCD
7, 2373–2412, 2013

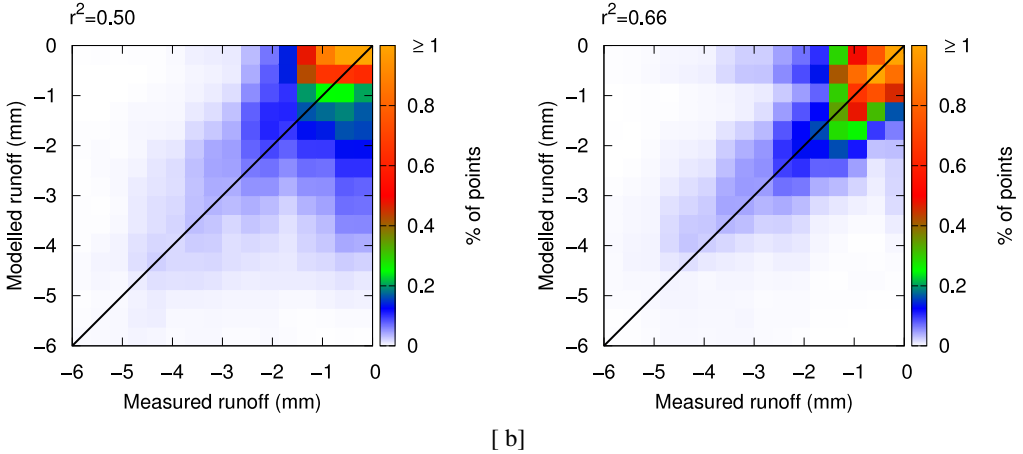

[a] [b]

Fig. 7. Density scatter plots for modelled versus measured runoff (mm) for the 1 h time scale for the bucket model **(a)** and RE (Yamaguchi) model **(b)**. In colour are shown the percentages in the specific region, cut off at 1 %.

TCD
7, 2373–2412, 2013